Application of the Pseudo Global Warming Dynamic Downscaling Method to the Tokai Heavy Rain in 2000

Journal of the Meteorological Society of Japan, Vol. 93, No. 5, pp. 551−570, 2015
DOI:10.2151/jmsj.2015-043

Application of the Pseudo Global Warming Dynamic Downscaling Method to the Tokai Heavy Rain in 2000

Kenji TANIGUCHI

Faculty of Environmental Design, Kanazawa University, Kanazawa, Japan

and

Kenjiro SHO

Department of Civil Engineering and Systems Management, Nagoya Institute of Technology, Nagoya, Japan

(Manuscript received 24 April 2014, in final form 14 July 2015)

Abstract

The Tokai region in central Japan often receives heavy rainfall because of typhoons. Furthermore, because of global warming, the intensity of heavy rainfall events is expected to increase in the future. Therefore, assessment of possible differences in such events between the present and future is important. In this study, a record heavy rainfall event in the Tokai region on 11 September 2000, the so-called Tokai Heavy Rain (THR), was numerically simulated by weather research and forecasting model with triple nesting grid system of 50-, 10-, and 2-km horizontal resolution. Simulated results present characteristics of rainfall and atmospheric conditions similar to the actual event. Thus, the simulation is considered valid for reproducing rainfall processes of the THR. In addition, variations of heavy rainfall events in future climate scenarios are investigated using numerical simulations based on pseudo global warming (PGW) conditions, constructed using third-phase results of Coupled Model Intercomparison Project multi-model global warming experiments. Under certain future climate scenarios, the Tokai region may experience heavy rainfall events in which maximum hourly rainfall and extent of heavy rainfall areas increases. Such variations are mainly attributed to increased specific humidity in the lower troposphere. In some PGW runs, there was no significant rainfall around the Tokai region. There was increased specific humidity in these runs, and the horizontal distribution of lower atmospheric air temperature was favorable for the formation of a mesoscale convergence zone, as seen in PGW runs with heavy rainfall. However, vertical profiles of equivalent potential temperature and saturated equivalent potential temperature showed unsaturated and stable atmospheric stratifications that are unfavorable for convective activity. Even in cases with increased atmospheric temperature and specific humidity caused by global warming, differences in their spatial distributions and vertical profiles could lead to contrasting effects of global warming on a specific extreme weather event.

Keywords climate change; heavy rainfall; dynamic downscaling; numerical simulation

1. Introduction

The Tokai region, on the Pacific side of central Japan, is often stricken by typhoon-induced heavy rainfalls and storm surges. In 1959, Typhoon Vera (typhoon Ise-wan in Japanese) struck the region,

Corresponding author: Kenji Taniguchi, Faculty of Environmental Design, Kanazawa University, Kakuma-machi, Kanazawa 920-1192, Japan
E-mail: taniguti@se.kanazawa-u.ac.jp

which includes Nagoya, one of the most heavily populated areas in Japan. The lowest central pressure of Vera was 929.5 hPa and the storm area expanded enormously. The maximum recorded instantaneous wind speed was 55.3 m s^{-1}, and an extraordinarily high storm surge overwhelmed dykes along the coast and at the river mouth. Typhoon Vera was one of the worst natural disasters to strike Japan and caused record damage in the region, with more than 5000 lives lost to high tides and floods.

Another heavy rainfall occurred in September 2000, which became known as the Tokai Heavy Rain (THR). This event was caused by the combined effects of a seasonal stationary front and typhoon, which produced record precipitation in the Tokai region. At the Tokai automated meteorological data acquisition system (AMeDAS) site on 11 September, the maximum hourly precipitation rate was 114 mm h^{-1} and daily precipitation was 492 mm, which is twice the mean monthly precipitation for September. River levels exceeded design water levels at many monitoring points of the Syonai and Shin rivers. There was widespread inundation within the protected area and bank failure increased the effect and depth of the flooding, which lasted for three days. Reports listed a death toll of 10 people and 23,896 houses affected by floodwater above floor level.

The THR was a typical flood event in the Tokai region. The combination of a typhoon near Japan and a weather front near the region often produces heavy rainfall around Aichi Prefecture. Similar patterns are found in heavy rain events during September 1983, 1991, 2004, and 2011. Maximum 3-hourly rainfall rates recorded in these events and that of the THR are among the 10 highest at the Nagoya AMeDAS site.

Variations of extreme weather events (tropical cyclones, typhoons, storms, and others) under global warming have been investigated. Studies of past tropical cyclones (TCs) based on observation results show that variations in the frequency of TC is ambiguous, but clear increase is recognized in the number of strong hurricanes in the late 20th century. Future variations of storms will be greater than that observed in the past, and significant increase in economic losses are expected (Pielke et al. 2005; Webster et al. 2005). In future climate conditions, examinations of global TC frequency show decreasing trends (Oouchi et al. 2006; Emanuel et al. 2008; Murakami et al. 2011; Kim et al. 2014). Variations in specific regions have also been investigated. There is an increasing trend of TC genesis in the central North Pacific, while a decreasing trend is observed in the western part (Yokoi and Takayabu 2009). Comparison of future variations in storm tracks between the northern and southern hemispheres shows poleward migration of tracks in both hemispheres, and frequency of extreme cyclones increases (decreases) in the southern (northern) hemisphere (Chang et al. 2012). In these works, increasing intensity of TCs or increasing number of extremely strong TCs are recognized. Some studies focus on precipitation from TCs and storms. Scoccimarro et al. (2014) made numerical experiments with three different idealized climate forcings to examine future precipitation variations in TC events. In the case of only warming in the atmosphere, precipitation and evaporation slightly decrease and precipitable water slightly increases. However, experiments with increasing sea surface temperature (SST) result in larger increase in precipitation, evaporation, and precipitable water content. Zappa et al. (2013) examined future variations in extratropical cyclones around the North Atlantic and European region. Although variations in wind speed were small, clear increasing tendencies of precipitation were found in future climate, and the tendency was greater in the high CO_2 emission scenario. Therefore, future heavy rain events around the Tokai region from typhoons might cause even more severe damage.

There have been a number of research works assessing the effects of global warming. Simulation output from coupled atmosphere-ocean global climate models (AOGCMs) are often used in studies of future climate. However, the spatial resolution of AOGCMs is generally several hundreds of kilometers, and the size of the Tokai region is about 200 × 200 km. Thus, AOGCM resolution is too coarse to investigate detailed changes in extreme heavy rain events. Therefore, even if a heavy rainfall event is found in a future climate scenario as an AOGCM result, detailed analysis is difficult. Smaller-scale predictions may be made using a dynamic downscaling (DDS) technique, which estimates higher-resolution climatic conditions in a physical model by considering detailed geographic information such as topography.

Sato et al. (2007) used a DDS method to model future changes of water resources in Mongolia. They calculated a 10-year mean difference between 20th-century and future climate runs by an AOGCM, and the difference was added to reanalysis data to create a forcing dataset for the DDS. This new forcing dataset is called a pseudo global warming (PGW) condition. A future DDS result of PGW forcing can be compared directly with a present DDS result from reanalysis data. Sato et al. (2007) showed that repro-

ducibility of the current climate in a DDS result with reanalysis data was superior to that of the original AOGCM output. Therefore, the DDS result of PGW forcing is expected to reflect the effects of global warming on the actual current climate.

Kawase et al. (2008; 2009) applied the PGW downscaling method to the Baiu rainband in Japan for a 40-day period, and then examined changes in the rainband system under future climates. In this manner, DDS with PGW forcing is helpful for studying a specific meteorological phenomenon. Kusaka et al. (2012) evaluated urban heating in future climates using the result of PGW downscaling with multiple AOGCM outputs. The targeted areas were Tokyo, Osaka, and Nagoya. Thus, the PGW downscaling method is useful for assessment of the effects of global warming at a city scale. Adaptation methods for climate change are expected to be implemented on a city scale. Thus, the PGW downscaling method for cities and detail assessment would be indispensable.

In the present study, the PGW downscaling approach of Sato et al. (2007) was applied to the THR. In Section 2, an overview of the dataset and design of the DDS with PGW forcing data are provided. In Section 3, results of THR simulation are discussed. In Section 4, the variation of heavy rainfall in future climates from the DDS with PGW conditions is investigated. In Section 5, atmospheric characteristics in the PGW runs are discussed. Finally, a summary is given in Section 6.

2. Method

2.1 Data

a. JRA55

Using reanalysis data, we performed control (CTL) simulations of the THR. Japanese 55-year Reanalysis product, JRA-55, from the Japan Meteorological Agency (JMA) was used. JRA-55 is produced by a system based on the low-resolution (TL319) version of JMA's operational data assimilation system, which has been extensively improved since the previous reanalysis (JRA-25). The atmospheric component of JRA-55 is based on the incremental four-dimensional variational method (Courtier et al. 1994). Newly available and improved past observations are used for JRA-55. Major problems in JRA-25 (cold bias in the lower stratosphere and dry bias in the Amazon) are ameliorated in JRA-55; therefore, there is improved temporal consistency of temperature. Further details are available in Kobayashi et al. (2015).

b. CMIP3 multi-model dataset

For assessment of future global warming, coordinated numerical experiments have been conducted by many modeling groups using state-of-the-art global coupled climate models under the framework of the Coupled Model Intercomparison Project (CMIP). In the present study, we used future climate projections of the third phase of CMIP (CMIP3; Meehl et al. 2007). The CMIP3 archive includes 3-hourly, daily, and monthly data. We used monthly mean output to prepare a PGW condition. Newer climate projections of the fifth phase of CMIP (CMIP5) have been published. The performance of AOGCMs in CMIP3 and CMIP5 are compared in the IPCC Fifth Assessment Report (IPCC 2013; hereafter, AR5). In AR5, some CMIP5 improvements are described, namely, simulation of clouds, storm track biases, monsoon characteristics, arctic ice extent, and others. However, there is no major improvement in some aspects (e.g., equatorial zonal wind, ocean heat transport, extreme temperature) and in interannual-to-interdecadal variability of certain teleconnections. Ranges of uncertainty in CMIP3 and CMIP5 are comparable, and their model performances are generally similar. Knutti and Sedláček (2013) showed that projected global temperature changes in CMIP3 and CMIP5 models are remarkably similar, and spatial patterns of temperature and precipitation are very consistent. It has also been shown that the mean and range of climate sensitivity and transient climate response of global mean temperature are similar in both CMIP3 and CMIP5 output (AR5; Knutti and Sedláček 2013). Therefore, there are similar uncertainties in both output; thus, the CMIP3 dataset is still useful in climate change studies.

In CMIP3, a scenario used for simulations of the present climate is called the 20th Century Climate in Coupled Models (20C3M; Nakicenovic and Swart 2000). However, the AOGCMs were used to quantify future climate changes using several possible emission scenarios. The future climate scenarios used in the present study are AOGCM outputs under the Special Report on Emissions Scenario A1B (Nakicenovic and Swart 2000).

Some organizations have produced multiple models. For example, two have been developed by the Geophysical Fluid Dynamics Laboratory of the National Oceanic and Atmospheric Administration (NOAA), two by the University of Tokyo and the National Institute of Environmental Studies in Japan, two by the National Center for Atmospheric Research, three by the Goddard Institute for Space Studies of

the National Aeronautics and Space Administration (NASA), and two by the UK Met Office (UKMO). Although these models often share components or parameterizations of subgrid-scale processes, they produce different results; therefore, each model was treated as independent in our study. A full list of the AOGCMs used is presented in Table 1. This table also shows anomalies of surface air temperature at 2 m above the surface. Values are differences between each PGW run and a CTL run around Japan (130–145°E, 30–45°N) for an average initial condition of the five ensemble members.

c. Sea surface temperature

For SST in the simulations, we used the NOAA Optimum Interpolation 1/4 Degree Daily Sea Surface Temperature Analysis (NOAA OI SST) (Reynolds et al. 2007). The NOAA OI SST dataset has a grid resolution of 0.25° and temporal resolution of 1 day. The product uses Advanced Very High Resolution Radiometer infrared satellite SST data. Advanced Microwave Scanning Radiometer SST data were also used after June 2002. In situ data from ships and buoys were included for large-scale adjustment of satellite biases.

d. Land-surface conditions

For the land-surface condition in the numerical simulations (volumetric soil moisture, soil temperature, soil type, and vegetation type), we used National Centers for Environmental Prediction (NCEP) Final Operational Global Analysis (NCEP FNL) data. NCEP FNL data are produced on a 6-hourly basis by the NCEP global data analysis system from July 1999 to a near-current date. Data spatial resolution is 1.0° × 1.0° (NCEP 2000).

e. Precipitation data for verification

For verification of the THR simulation, two precipitation datasets were used. To investigate the spatial distribution of precipitation around Japan, we used data from the Global Precipitation Climatological Project (GPCP). GPCP data are derived from a merged analysis of satellite microwave data, geosynchronous-orbit satellite infrared data, and surface rain gauge observations. Daily precipitation is available from 1997 onward (Huffman et al. 2001) with a spatial resolution of 1.0° × 1.0°.

To examine the detailed distribution of precipitation around the Tokai region, simulated results were compared with a product combining weather radar data and in situ observations from the JMA AMeDAS network. This dataset, the so-called Radar-AMeDAS, is important in observation and warning of heavy rainfall. Radar-AMeDAS data have high temporal and spatial resolutions (1 hour and 5 km for data from 2000, respectively). Therefore, Radar-AMeDAS precipitation (RAP) data are suitable for verification of the temporal variation and spatial distribution of modeled precipitation.

2.2 Pseudo global warming conditions

A THR simulation was conducted as the CTL. This was performed with initial and boundary conditions prepared from JRA-55, NCEP FNL, and NOAA 0.25 interpolated OI SST. PGW conditions of THR were calculated from future and present climate conditions. Future climate conditions were obtained as the 10-year monthly mean from 2061 to 2070 under the Special Report on Emissions Scenario A1B in one ensemble of the CMIP3 model output. Present climatic conditions were obtained as the 10-year monthly mean from 1991 to 2000 in 20C3M. Then, anomalies of global warming were considered as the difference between future and present climatic conditions. These anomalies were added to 6-hourly atmospheric conditions of the THR from JRA-55. Thus, a set of PGW conditions is constructed for wind, atmospheric temperature, geopotential height, surface pressure, and specific humidity. For relative humidity, original values in JRA-55 were retained in the PGW conditions, and specific humidity in these conditions was defined from the relative humidity and modified atmospheric temperature of the future climate. To prepare SST for the PGW condition, the SST anomaly obtained from future and present climate conditions in CIMP3 output was added to the NOAA SST.

In addition to CTL, we performed simulations with PGW forcing prepared using 11 different CMIP3 data. A list of the CMIP3 data used and their abbreviations are given in Table 1. Hereafter, using the numbers in Table 1, runs with PGW conditions are labeled PGW-1 through PGW-11.

2.3 Design of numerical simulations

For DDS of future and present climate conditions, numerical weather prediction or regional climate models are typically used. In the present study, weather research and forecasting model version 3.5.1 (Skamarock et al. 2008) was adopted for the CTL and PGW runs. A two-way triple nesting grid system was used, as shown in Fig. 1. The coarsest domain (D01) was centered on the Tokai region with 50-km horizontal resolution, covering an area from the eastern

Table 1. CMIP3 model outputs used in this study.

	IPCC ID	Institute and Country	Resolution	Mean anomaly of initial surface air temperature in D01 (Kelvin)
1	CGCM3.1(T47)	Canadian Center for Climate Modeling and Agency (Canada)	T47 L31	2.09
2	CGCM3.1(T63)		T63 L31	1.78
3	CNRM-CM3	Meteo-France, Centre Nationale de Recherches Meteorologique (France)	T42 L45	2.21
4	GFDL-CM2.1	US Dept. of Commerce / NOAA / Geophysical Fluid Dynamics Laboratory (USA)	144x90 L24	2.35
5	GISS-AOM	NASA/Goddard Institute for Space Studies (USA)	72x46 L17	1.44
6	GISS-EH		90x60 L12	1.73
7	ECHAM5/MPI-OM	Max Planck Institute for Meteorology (Germany)	T63 L32	2.25
8	INM-CM3.0	Institute of Numerical Mathematics (Russia)	72x45 L21	2.24
9	MIROC3.2(hires)	Center for Climate System Research (the University of Tokyo), National Institute for Environmental Studies, and Frontier Research Center for Global Change (Japan)	T106 L56	3.53
10	MRI-CGCM2.3.2	Meteorological Research Institute (Japan)	T42 L30	2.21
11	UKMO-HadGM1	Hadley Center for Climate Prediction and Research, Met Office (UK)	N96 L38	2.74

edge of the Eurasian continent to the northwestern Pacific. Intermediate and finest resolution domains (D02 and D03) covered most of the main island of Japan and Tokai region, with horizontal resolutions 10 and 2 km, respectively. All three domains had 35 vertical layers, and the top of the model atmosphere was 20 hPa.

Ensemble simulations with different initial conditions were performed for the CTL and each PGW condition. To attain different initial conditions, the lagged average forecast (LAF) method of Hoffman and Kalnay (1983) was used. In LAF, multiple simulations beginning at different initial times are performed, and a set of ensemble forecasts is obtained. Therefore, differences between the CTL and PGW runs could be examined, and it could be determined whether they are attributable to effects of global warming or chaotic variations among the ensemble members. Five members for each ensemble were set up with 6-hour lags. Members began at 21:00 JST on 9 September 2000, and 03:00, 09:00, 15:00, and 21:00 JST on 10 September. They terminated at 21:00 JST on 12 September. A summary of ensemble members and their members is shown in Table 2.

The Betts–Miller–Janjic cumulus parameterization (Janjic 1994, 2000) and Morrison double-moment microphysics parameterization schemes (Morrison et al. 2009) were used to calculate precipitation in the model. For D03, cumulus parameterization was not applied. Physical processes of the surface layer, boundary layer, and land surface were calculated by the Eta model based on Monin–Obukhov with Zilitinkevich thermal roughness length (Zilitinkevich 1995), Bretherton and Park scheme (Bretherton and Park 2009), and Noah land surface model (Chen and Dudhia 2001), respectively. For longwave and shortwave radiation, we used the rapid radiative transfer model with the Monte Carlo independent column approximation method of random cloud overlap (Iacono et al. 2008). For D01, a spectral nudging method was used for atmospheric temperature, zonal wind, meridional wind, and geopotential height every 6 hours, above a height of 6 – 7 km. Model settings are given in Table 3.

3. Results of control run

Figure 2 shows distributions of total precipitation during 10 – 12 September 2000 in D01. GPCP rainfall shows precipitation from Okinawa throughout the main island of Japan (Fig. 2). Similar patterns of precipitation were recognized in the results of the ensemble members of CTL. Around the Tokai

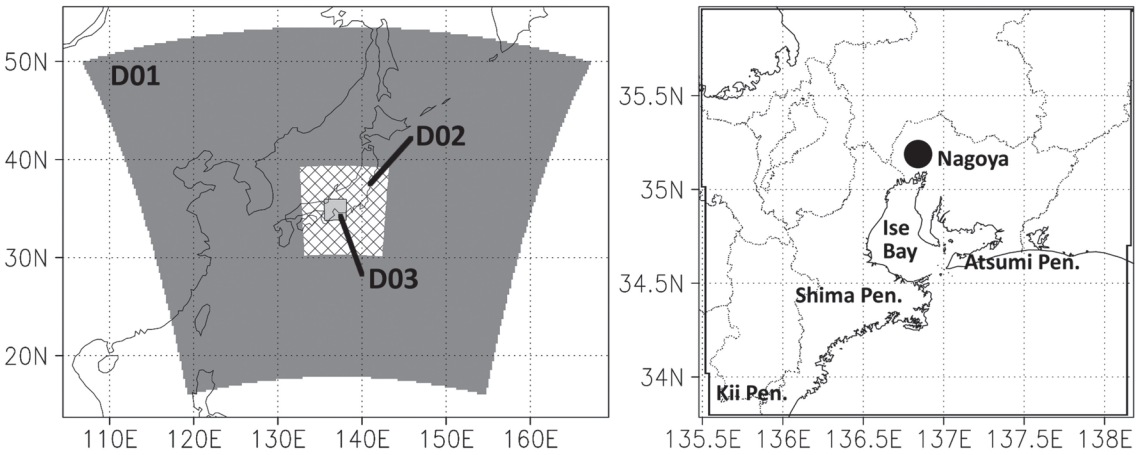

Fig. 1. Target domains of downscaling in weather research and forecasting (WRF). Areas indicated by darker shade, cross-hatching, and lighter shade are D01, D02, and D03, respectively. The spatial resolutions are 50, 10, and 2 km for D01, D02, and D03, respectively.

Table 2. Summary of ensemble members

Ensemble Name	Simulation Period	Lag hours from ENS1
ENS1	09:00JST 10 Sep. – 21:00JST 12 Sep.	0 hours
ENS2	21:00JST 9 Sep. – 21:00JST 12 Sep.	−12 hours
ENS3	03:00JST 10 Sep. – 21:00JST 12 Sep.	−6 hours
ENS4	15:00JST 10 Sep. – 21:00JST 12 Sep.	+6 hours
ENS5	21:00JST 10 Sep. – 21:00JST 12 Sep.	+12 hours

Table 3. WRF settings

Version of model	V3.5.1
Cloud microphysics	Morison double-moment
Cumulus parameterization	Betts-Miller-Janjic Scheme (no cumulus parameterization for D03)
Long- and short-wave radiation	RRTMG Scheme
Land surface scheme	Eta model
Land model	Noah Land Surface Model
Planetary boundary layer scheme	Bretherton and Park Scheme
Settings of spectral nudging	Applied to the layer above 6 – 7 km for atmospheric temperature, zonal and meridional wind, geopotential height

region, heavy rainfall is shown by the GPCP. In the eastern part of the main island, rainfall tended to be underestimated in the CTL results. Spatial correlations and root mean square deviations (RMSDs) of total precipitation in D01 were calculated between the results of ENS1 and other ensemble members (Table 4). Figure 2 shows that the spatial distribution of precipitation among members in the CTL is similar, with spatial correlations > 0.8. Table 5 shows total rainfall averages for D01. Values are from 10 to 12, and their deviations from the average are less than 10 %. Although initial conditions varied among the ensemble members, they did have some similarity.

Figure 3 is the same as Fig. 2, but for D03 and RAP. RAP shows heavy precipitation with total rainfall > 700 mm over the eastern Kii and Shima peninsulas. To the south of Nagoya, there is also a heavy precipitation area extending from the southwest to the northeast.

The CTL results also show heavy rainfall areas

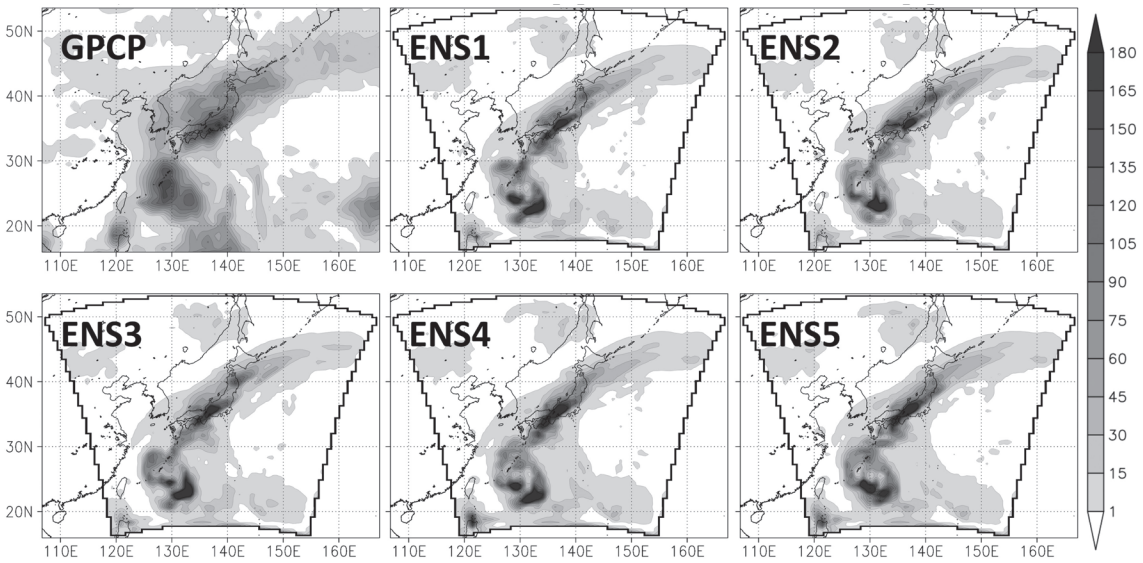

Fig. 2. Spatial distribution of total precipitation during 10–12 September for GPCP, and from 21 JST 10 September to 21 JST 12 September in D01 for each ensemble member of CTL. Color bar shows rainfall (mm).

Table 4. Spatial correlations and root mean square deviations of total precipitation in D01 between ENS1 and other four ensemble members (ENS2-5)

	Spatial correlation vs ENS1					RMSD vs ENS1 (mm)				
	ENS2	ENS3	ENS4	ENS5	Avg.	ENS2	ENS3	ENS4	ENS5	Avg.
CTL	0.83	0.92	0.92	0.89	**0.90**	16.0	11.5	11.7	13.7	**13.2**
PGW-1	0.82	0.94	0.90	0.84	**0.88**	18.9	11.4	14.5	18.2	**15.7**
PGW-2	0.75	0.88	0.90	0.87	**0.85**	22.5	15.6	16.2	16.8	**17.8**
PGW-3	0.78	0.84	0.80	0.80	**0.80**	21.1	18.2	20.9	21.3	**20.4**
PGW-4	0.76	0.86	0.92	0.87	**0.85**	23.8	19.0	14.4	17.7	**18.7**
PGW-5	0.74	0.87	0.91	0.85	**0.85**	23.7	16.5	14.5	18.0	**18.2**
PGW-6	0.78	0.93	0.90	0.89	**0.86**	22.6	18.0	15.9	16.5	**18.3**
PGW-7	0.88	0.93	0.88	0.83	**0.88**	16.8	12.7	17.2	20.0	**16.7**
PGW-8	0.79	0.93	0.74	0.88	**0.83**	20.8	12.7	15.5	16.2	**18.8**
PGW-9	0.84	0.89	0.87	0.80	**0.85**	18.8	15.5	17.3	21.2	**18.2**
PGW-10	0.85	0.89	0.93	0.87	**0.89**	16.3	14.6	11.5	15.7	**14.5**
PGW-11	0.80	0.90	0.92	0.80	**0.86**	23.2	16.7	14.6	22.8	**19.3**

extending from the southwest to the northeast. However, the location of these areas is north of those from RAP. In the ENS2 and ENS5 results, areas of precipitation > 700 mm are recognized, but the heavy rainfall areas are smaller than those from RAP. Rainfall distributions in the other three ensemble members are similar to RAP, but amounts are much smaller. In D01, spatial distributions and rainfall amount are similar among the ensemble members, but there are significant differences in a limited region such as D03.

Figure 4 (upper panels) shows sea level air temperature, wind vectors at 10 m above the surface, and hourly precipitation in D03 for ENS1 of the CTL. Here, sea level air temperatures are modified values of air temperature at 2 m above the surface. This modification used a temperature lapse rate of 0.65 K/100 m. At 17:00 JST on 11 September, there was a southeasterly wind in the southeast part of D03. This wind direction corresponds to the radiosonde observation shown in Watanabe (2002). This wind provided warm,

Table 5. Mean total rainfall in D01 and D03 for ensemble members and their averages

	Mean Total Rainfall in D01 (mm)						Mean Total Rainfall in D03 (mm)					
	ENS1	ENS2	ENS3	ENS4	ENS5	**Avg.**	ENS1	ENS2	ENS3	ENS4	ENS5	**Avg.**
CTL	11.3	10.4	10.9	11.7	11.6	**11.3**	124.9	156.5	161.3	133.2	111.3	**137.4**
PGW1	12.7	11.8	12.4	13.1	12.6	**12.5**	86.7	121.7	173.0	111.7	97.5	**118.2**
PGW2	12.4	11.2	11.9	12.6	12.4	**12.1**	142.4	192.5	188.4	123.5	124.5	**154.3**
PGW3	12.4	12.2	12.7	13.3	13.2	**12.8**	133.0	190.0	192.9	138.5	133.6	**157.6**
PGW4	12.8	11.5	12.3	13.0	12.6	**12.4**	149.0	138.4	145.6	115.4	146.8	**139.0**
PGW5	13.1	12.1	12.7	13.5	13.1	**12.9**	122.1	133.5	133.4	102.6	56.5	**109.6**
PGW6	13.0	11.7	11.3	13.1	12.6	**12.5**	131.7	151.7	132.7	143.3	138.3	**139.5**
PGW7	12.4	11.3	11.9	12.5	12.1	**12.1**	194.2	210.6	227.8	158.9	121.5	**182.6**
PGW8	13.0	11.9	12.4	13.0	12.8	**12.6**	123.5	106.5	89.4	119.9	93.5	**106.6**
PGW9	14.4	13.4	13.8	14.4	14.0	**14.0**	22.6	43.9	41.5	25.0	29.9	**32.6**
PGW10	13.3	12.5	12.9	13.4	13.3	**13.1**	59.4	73.1	44.1	62.0	54.1	**58.5**
PGW11	12.7	11.6	12.3	12.6	12.2	**12.3**	16.5	16.3	23.8	22.4	28.3	**21.5**

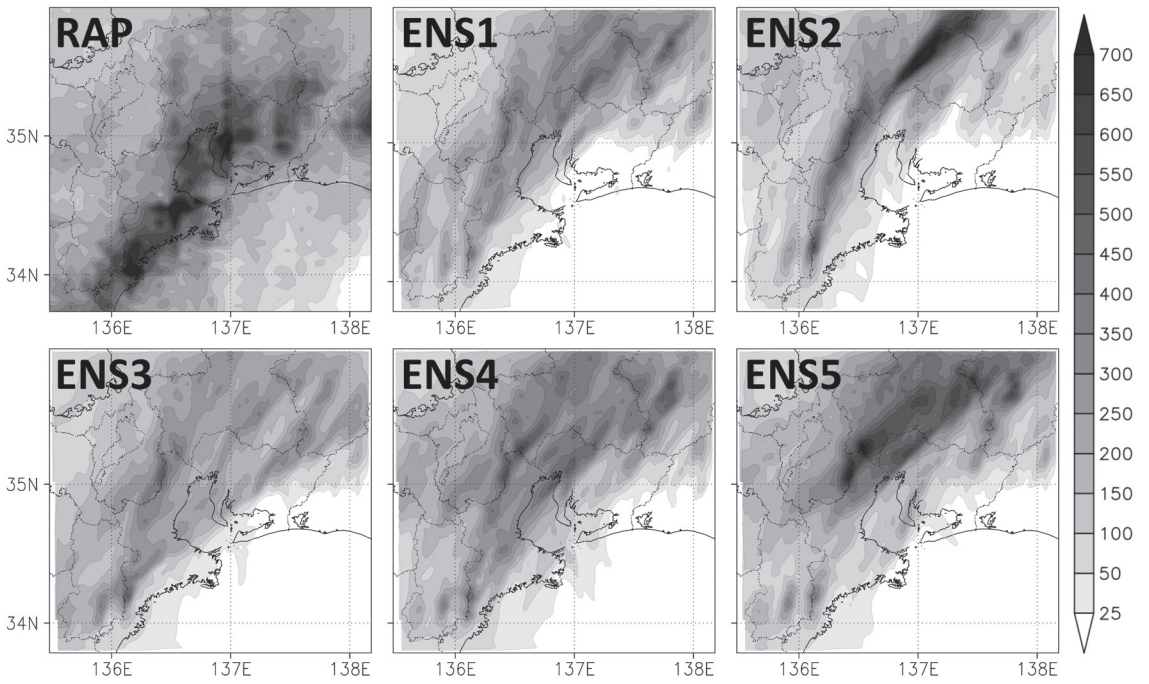

Fig. 3. Spatial distribution of total precipitation by Radar-AMeDAS and each ensemble member of CTL from 21 JST 10 September to 21 JST 12 September. Color bar shows rainfall (mm).

moisture-laden air during the THR (Watanabe 2002). Air temperature was cooler on land than in coastal and ocean areas, and heavy rainfall was recognized in the zone of large temperature gradient. At 19:00 and 21:00 JST on 11 September, when the area of heavy rain moved eastward, a rainband formed where the cold air mass met the warmer air. These results indicate that formation of a frontal system caused heavy rain. The associated temperature distribution and motion of the convergence zone (or rainband) were recognized by surface observations (Watanabe 2002). There was a southwesterly wind at 500 hPa across a wide area of D03 (Fig. 4, lower panels). This wind direction corresponds approximately to the direction

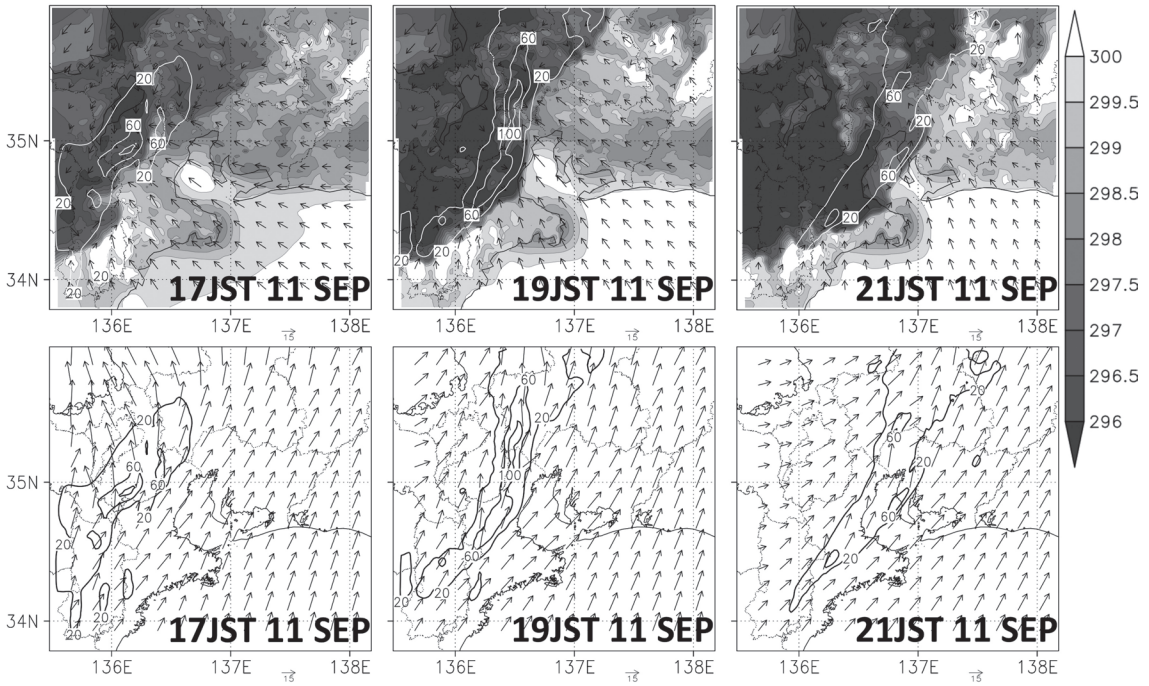

Fig. 4. Upper panels: temporal variation of spatial distributions of sea-level air temperature, wind vectors 10 m from the surface, and hourly precipitation in D03 of control run, from 17 JST 11 September to 21 JST 12 September. Lower panels: wind vectors at 500 hPa and precipitation. Results are for every 2 hours. Gray shading indicates air temperature and thick contours precipitation. Color bar shows temperature (K).

of the rainband. The same characteristics are found in the radiosonde observation (Watanabe 2002) and RAP. Thus, the THR is assumed to be a back- and side-building type of rain system (Kato 2002). The aforementioned characteristics in rainfall distribution and atmospheric conditions indicate that mechanisms of heavy rainfall in THR were successfully reproduced by the CTL, though simulated areas and amounts of rain are different from the actual THR (Fig. 3). In the other four ensemble members of the CTL, we also discovered these characteristics (inflow of warm and moist air in the lower layer, distributions of surface air temperature and convergence zone, and southwesterlies in the mid-troposphere), showing that these runs also reproduced the THR mechanism well (figures not shown).

4. Results of pseudo global warming experiments

4.1 Rainfall around Japan

We generated the PGW conditions from initial and boundary conditions of the CTL run following the method of Sato et al. (2007), as described in Section 2.2. Eleven AOGCMs of CMIP3 shown in Table 1 were used to produce these PGW conditions.

Figure 5 shows spatial distributions of total rainfall in D01 over 2 days from 21:00 JST on 10 September, in ENS1 of the 11 PGWs. A rainfall area extending southwest to northeast over Japan as seen in the CTL is recognized in all PGW runs. Especially in PGW-1 through PGW-8, this heavy rainfall area is over the Tokai region. In PGW-10, although the overall rainfall distribution is similar to the CTL, only weak rainfall was recognized in the Tokai region. In PGW-9 and PGW-11, the heavy rainfall area shifts to the north of that region. Figure 6 is the same as Fig. 5, but for ENS2 through 5 of PGW-1 and PGW-11. In all four ensemble members of the PGW-1, a heavy rainfall area is evident over the Tokai region, as seen in ENS1 of PGW-1. Similarly, in all four ensemble members of PGW-11, the heavy rainfall area shifts northwestward to the Sea of Japan side, as seen in ENS1 of PGW-11. Spatial correlations of total precipitation between ENS1 and the other four ensemble members exceed 0.8 and RMSDs from ENS1 are reasonably small in both PGW-1 and PGW-11 (Table 4). The results in Fig. 6 and Table 4 show that variations in rainfall

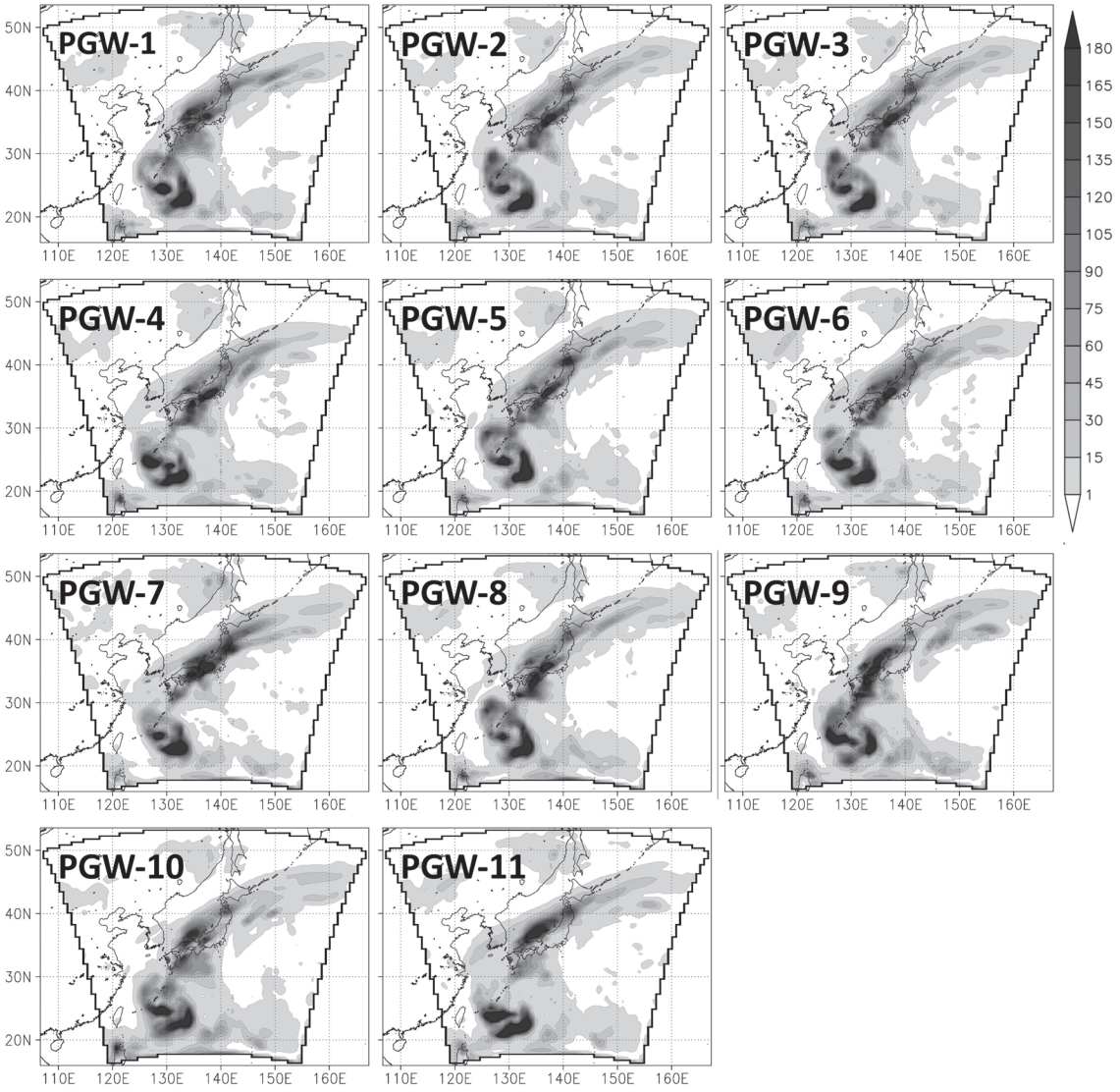

Fig. 5. Spatial distributions of total precipitation in D01 from 21 JST 10 September to 21 JST 12 September for ENS1 of 11 PGW runs. Color bar shows rainfall (mm).

patterns were similar among ensemble members in PGW-1 and PGW-11. Table 4 also shows that spatial correlations and RMSDs for PGW-2 through PGW-10 are comparable to the CTL, PGW-1 and PGW-11. Not only such statistics but also visual comparisons of spatial patterns of total precipitation in each PGW simulations reveal similar patterns among ensemble members (figures not shown). These results indicate that chaotic behavior caused by perturbed initial conditions is small in our simulations, and it is expected that differences in spatial precipitation pattern between the CTL and each PGW run are caused by global warming.

Table 5 lists mean total rainfalls in D01 for all simulations. Averages from PGW-1 through PGW-11 are larger than those from CTL ensemble members. In addition, values from each ensemble member of PGWs are larger than the same ensemble members of the CTL. In the PGW conditions created from JRA55 and each AOGCM output, the same relative humidity is found but with a warmer atmosphere. Thus, specific humidity of future climate in PGW conditions

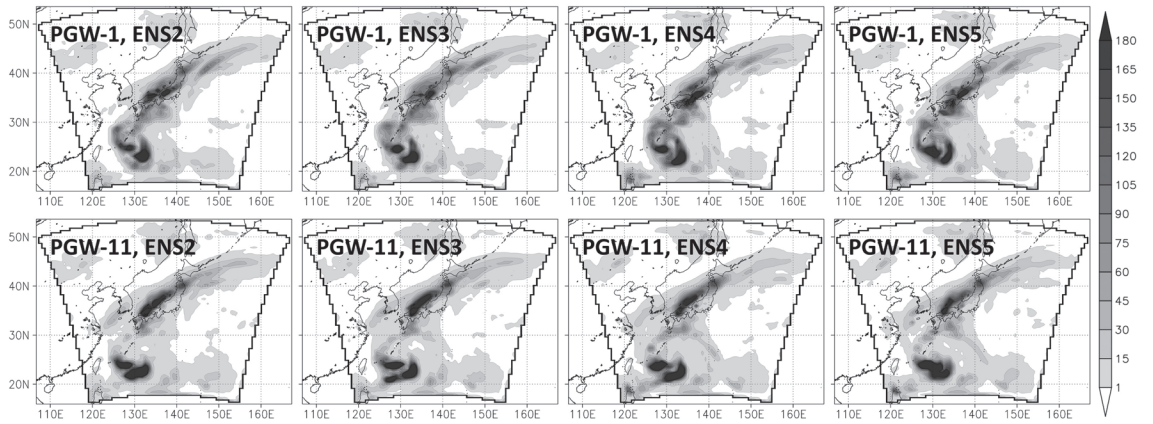

Fig. 6. Same as Fig. 5 but for ENS2 to ENS5 and PGW-1 and PGW-11. Color bar shows rainfall (mm).

increased. Such atmospheric variations can augment mean total rainfall.

In PGW runs, precipitation variations caused by a typhoon were distinguished. In some runs (PGW-5, PGW-6, PGW-8 and PGW-9), heavy rainfalls around southern Kyushu Island increased. Variations of typhoon activity in PGW runs are of great interest, but they were not a focus of the present study.

In numerical simulations, changes of initial and boundary conditions sometimes create problems. However, the results in Fig. 5 do not show unrealistic behaviors along boundaries, and precipitation amounts are comparable to the CTL results. Therefore, the PGW method did not cause critical errors in the simulations.

4.2 Heavy rainfall in Tokai region

Maximum total rainfalls in D03 are shown in Fig. 7 for the CTL and each of the 11 PGW runs. The average of these rainfalls from five ensemble members of the CTL is ~600 mm. For PGW-1 through PGW-8, in which the heavy rain areas are around the Tokai region, averages of maximum total rainfalls are 500–700 mm, and there were no significant differences in the ranges of ensemble members between the CTL and each PGW run. There may not be a clear effect of global warming on maximum total rainfall in the heavy rain areas under atmospheric conditions similar to THR. For PGW-9 through PGW-11, values are significantly smaller than the CTL, because the heavy rain area shifts mostly outside D03 in these cases. The numbers of grids with total rainfall > 400 mm are shown in Fig. 7 (the D03 grid is 120 × 120). In PGW-9, PGW-10, and PGW-11, areas of rain > 400 mm were very small or nonexistent. In other PGWs and the CTL, there were significant differences between ensemble members. Average values are larger than the CTL in some PGWs and smaller in others. Overall, there was no clear tendency in variation of total rainfall and extent of heavy rainfall areas for THR-type heavy rain under the global warming conditions.

Figure 8 presents locations of maximum hourly rainfall in all ensemble members from the CTL and PGW runs. Maximum hourly rainfall from each member is also shown. The observed maximum hourly rainfall was 114 mm h^{-1} at the Tokai AMeDAS station (south of Nagoya). The CTL results indicate maxima of 110.6–153.2 mm h^{-1}, with locations in western Nagoya from multiple ensemble members.

In PGW-5 and PGW-6, maximum hourly precipitation was near Nagoya. In other PGW runs, locations of maximum hourly rainfall were scattered across D03. For PGW-1 through PGW-8, in which the heavy rain areas were around the Tokai region in D01, all maxima were > 100 mm h^{-1}. In PGW-9, PGW-10, and PGW-11, the maxima are smaller than other PGWs, because the heavy rain areas are displaced northward (Fig. 5). Although the distributions of maximum hourly rainfall differed between runs, there have been heavy rain events similar to each PGW run in the past; thus, the results are considered realistic. Therefore, rainfall events similar to the PGW runs may occur in future climate.

Maximum hourly rainfalls in D03 are compared between the CTL and PGW runs in Fig. 9. Averages from many PGW runs are larger than from the CTL, with heavy rain around the Tokai region (PGW-1

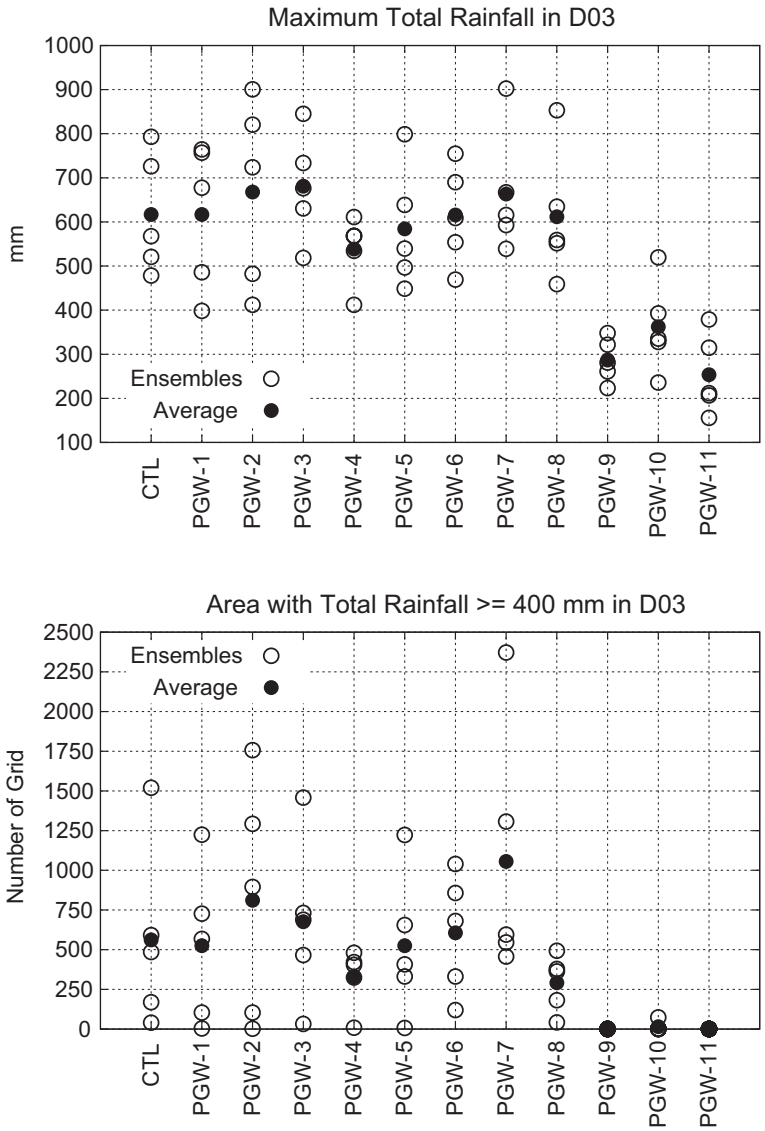

Fig. 7. Upper panel: maximum total rainfall in D03 during 21 JST 10 September through 21 JST 12 September for all ensemble members and their average in CTL and PGW runs. Vertical axis is rainfall (mm). Lower panel: number of grids with total rainfall > 400 mm in D03. Open circles indicate results for ensemble members and filled circles for averages.

through PGW-6 and PGW-8). Results of the *F*-test show homoscedasticity between the CTL and these PGW runs. In PGW-9, PGW-10, and PGW-11, which are the cases with northward shift of heavy rain areas, averages are smaller than in the CTL, although some values are >100 mm h^{-1}. Even outside the heavy rain area, there were some concentrated heavy rainfalls over a short period. Numbers of grids with maximum hourly rainfall > 70 mm h^{-1} are shown in Fig. 9 (D03 grid size = 120 × 120). The results reveal large variations among ensemble members. However, in many PGWs with heavy rainfall around the Tokai region (PGW-1 through PGW-4 and PGW-6), averages exceeded those in the CTL. Regarding hourly rainfall not only can maxima increase in the future but areas of concentrated heavy rainfall can also increase over a short period.

Table 5 lists mean total rainfalls in D03 from all

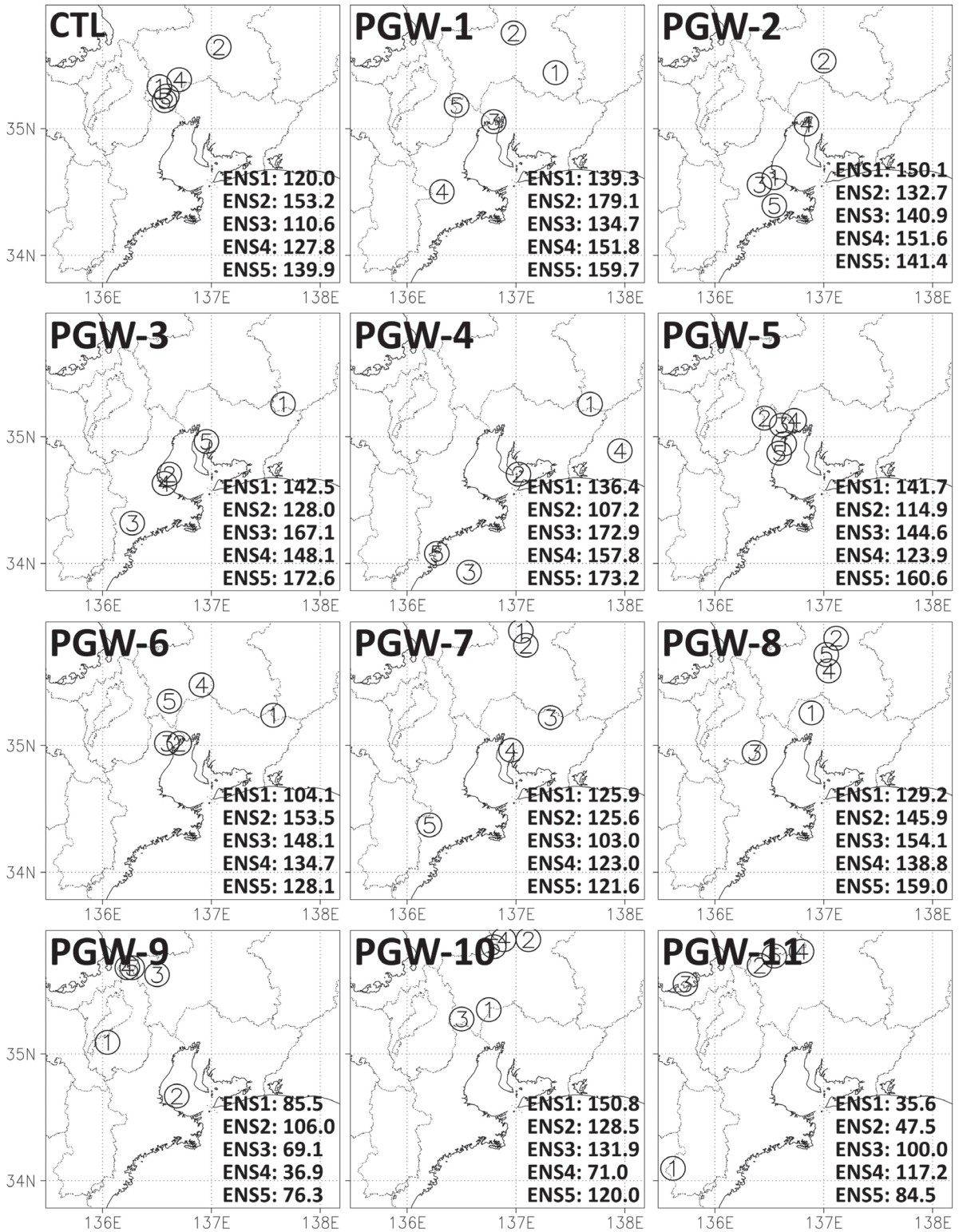

Fig. 8. Locations of maximum hourly rainfall in D03 for all ensemble members in CTL and PGW runs. Values indicate maximum hourly rainfall in D03 for each simulation.

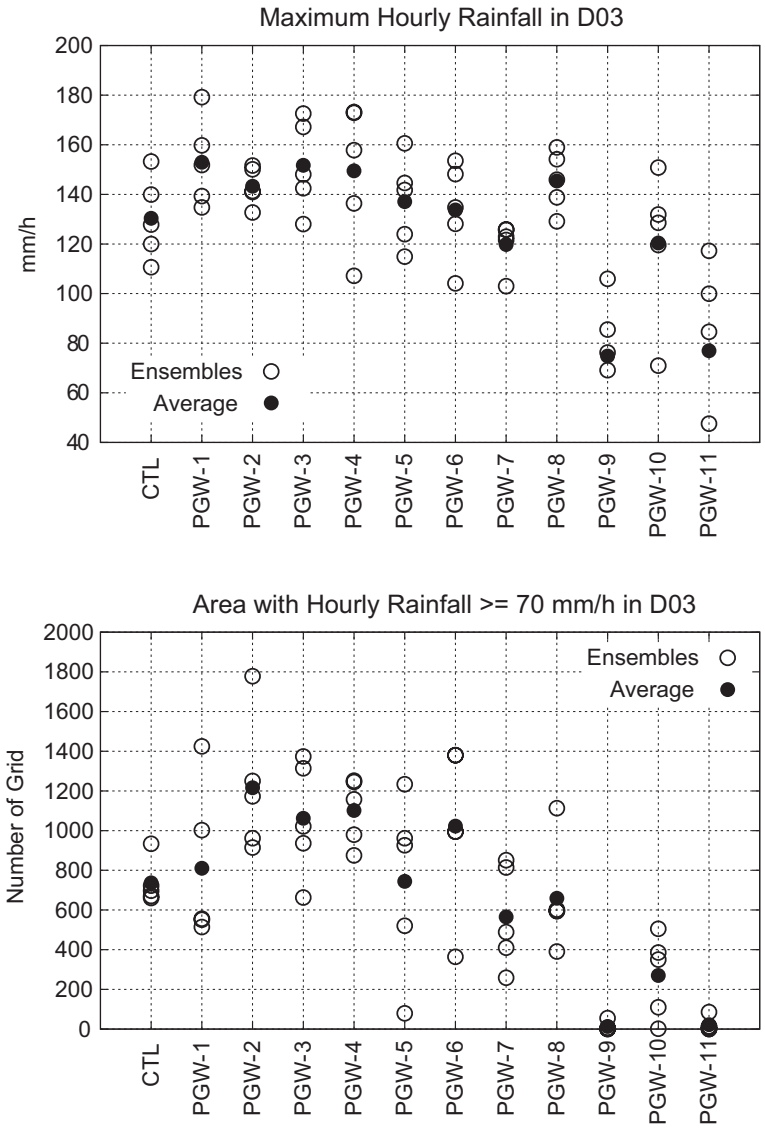

Fig. 9. Upper panel: maximum hourly rainfall in D03 for all ensemble members and their average in CTL and PGW runs. Unit of vertical axis is mm h^{-1}. Lower panel: number of grids with maximum hourly rainfall > 70 mm h^{-1} in D03 for all ensemble members and their average in CTL and PGW runs. Open circles indicate results for ensemble members and filled circles for averages.

simulations. These rainfalls increased in D01 but there was no clear tendency in D03, even for the heavy rainfall around the Tokai region (PGW-1 through PGW-8). The D03 results indicate that heavy rainfall over a short period can intensify, but its duration may not increase in THR-type rainfall under the global warming condition.

5. Comparison of atmospheric conditions between present and future climate

As seen in Section 4, heavy rainfalls such as the THR are produced in future climate, and some results indicate that concentrated heavy rainfall could intensify. Nevertheless, some PGW runs produced an absence of heavy rainfall around the Tokai region.

Figure 10 presents spatial distributions of 850 hPa

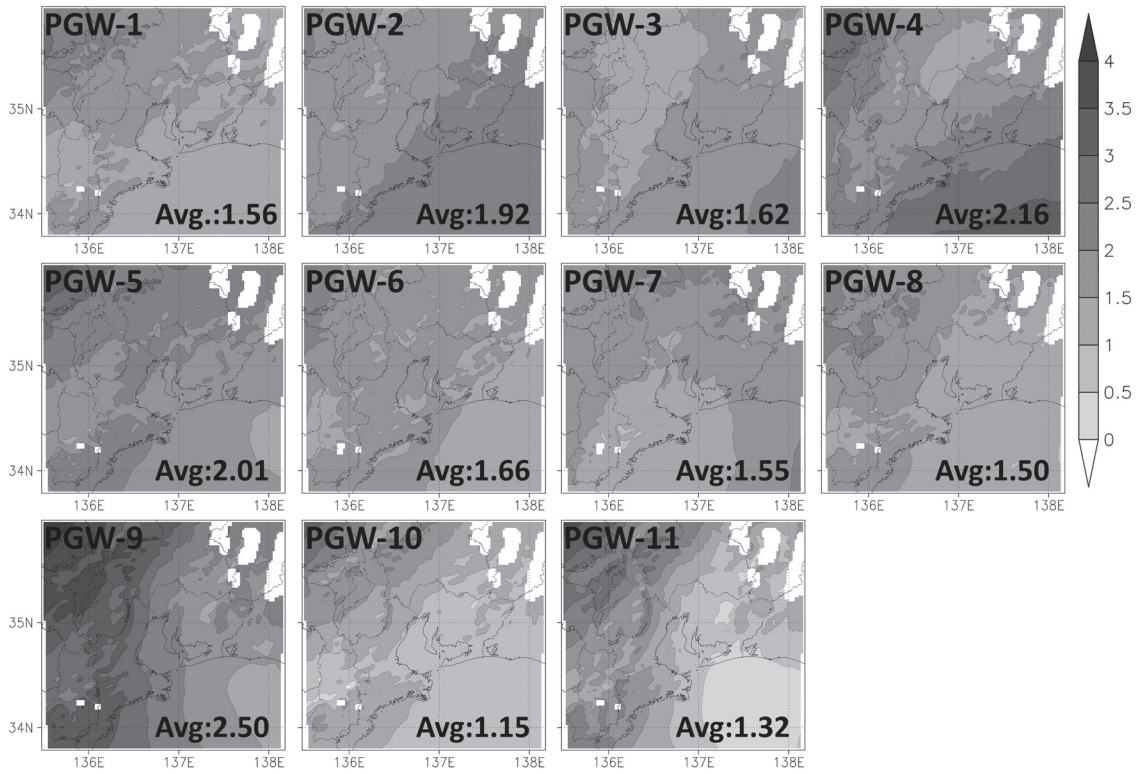

Fig. 10. Spatial distributions of difference in 850 hPa specific humidity between each PGW and CTL. Results are averaged for the period from 15:00 JST 11 September to 09:00 JST 12 September and five ensemble members. Color bar shows humidity (g kg^{-1}). Spatial mean value is also shown for each PGW.

specific humidity difference between the CTL and PGW runs. Values were averaged between ensemble members from 15:00 JST on 11 September to 09:00 JST on 12 September. In all PGW runs, specific humidity increased in D03. In PGW-10 and PGW-11, the spatial average of increased specific humidity was smaller than the others, and this might be a cause of reduced rainfall around the Tokai region. Conversely, there was a greater increase in PGW-9, which generated little rainfall around that region. Increasing specific humidity enhances precipitable water in the atmosphere, which can intensify heavy rainfall. However, more water vapor supply in the PGW runs did not necessarily reproduce heavy rainfall events. Thus, increasing water vapor alone cannot prolong rainfall events.

Figure 11 shows the spatial distribution of air temperature anomaly at 850 hPa from the CTL and PGW runs. The anomaly is calculated as the difference of temperature at each grid and the spatial mean around Ise Bay (136.5°–137.0°E, 34.5°–35.0°N). The CTL result shows cooler air temperature over land than in the Ise Bay area and formation of a linear temperature gradient zone to the west of that bay. These temperature gradients are important for the formation of a frontal convergence zone, which produces heavy rainfall. In PGW runs, air temperature over land was cooler than near Ise Bay, and there were similar patterns of temperature gradient to the west of the bay. Even in the PGW runs lacking heavy rainfall around the Tokai region (PGW-9, PGW-10, and PGW-11), there were patterns similar to the heavy rainfall cases. These results indicate that the absence of heavy rainfall around the Tokai region in future climate is not caused by changes in lower tropospheric temperature.

Figure 12 displays the spatial distribution of relative humidity at 850 hPa from the CTL and difference of relative humidity between each PGW run and the CTL. Values were averaged between ensemble members from 15:00 JST on 11 September to 09:00 JST on 12 September. In the CTL, mean relative

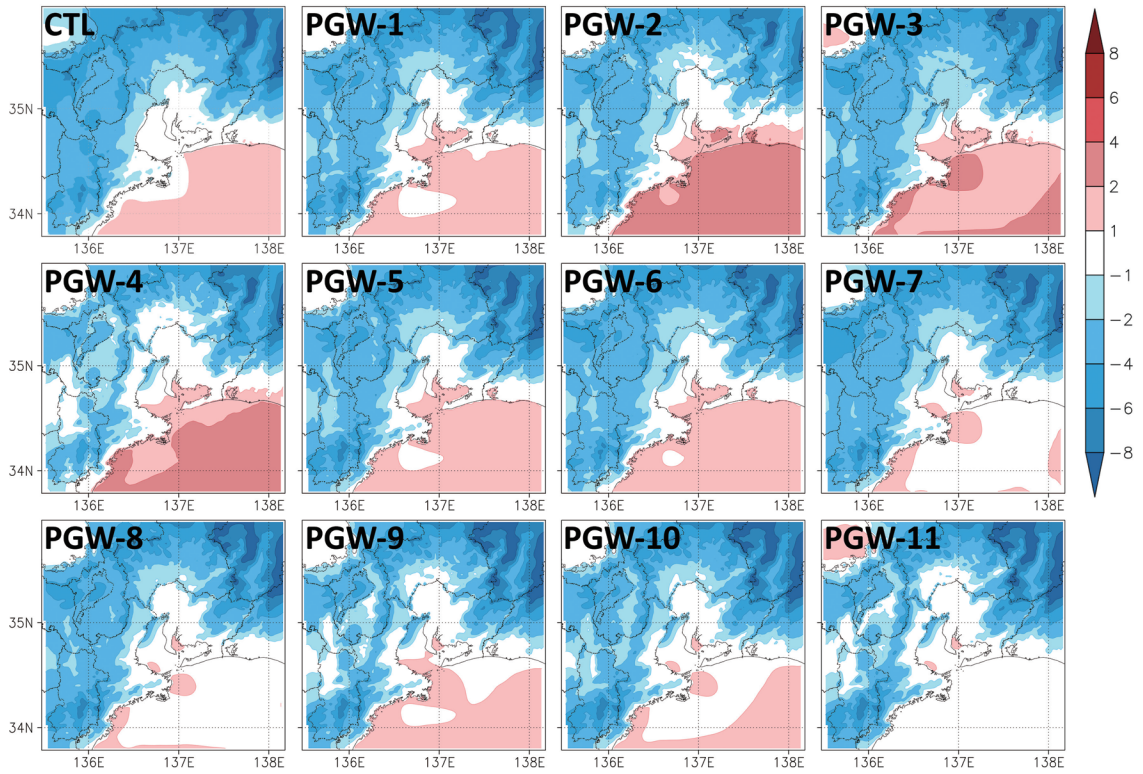

Fig. 11. Spatial distribution of 850 hPa air temperature anomaly for CTL and PGW runs. Anomaly is calculated as the difference of temperature at each grid and spatial mean around Ise Bay (136.5°–137.0°E, 34.5°–35.0°N). Results are averaged over the period from 15:00 JST 11 September to 09:00 JST 12 September and five ensemble members. Color bar shows temperature (K).

humidity was > 95 % across a wide area of D03. In PGW-1 through PGW-8, differences in relative humidity were small, and relative humidity was as high as that in the CTL. In the PGW runs with no rainfall around the Tokai region, relative humidity was less across a wide area of D03. Even if specific humidity increases in future climate (Fig. 10), atmospheric temperature also rises. Thus, relative humidity does not necessarily increase.

Figure 13 shows vertical profiles of potential temperature (θ), equivalent potential temperature (θ_e), and saturated equivalent potential temperature (θ_e^*) averaged between five ensemble members in the CTL and PGW runs. The results are spatial means in the area of 136.2°–137.7°E, 34.6°–35.4°N. In all results, the lower the atmospheric layer, the smaller the θ; however, θ_e showed conditionally unstable profiles in all runs. In the CTL, θ_e and θ_e^* were similar from 850 to 600 hPa, indicating that the atmosphere could become unstable and convection could readily occur. From PGW-1 through PGW-8, θ_e and θ_e^* were similar, as seen in the CTL. However, the difference between θ_e and θ_e^* in the other three PGW runs was greater than in those with heavy rainfall around the Tokai region. In these PGW runs, relatively stable conditions formed around the region and convective activity was suppressed.

In PGW-9, PGW-10, and PGW-11, the stable profiles are believed to be the reason for the absence of heavy rain around the Tokai region. Figures 10 and 11 show that under conditions of global warming, the temperature gradient can be similar to that in the present climate and that specific humidity will increase. The occurrence of similar heavy rain events and increasing rain amounts is presumed to be from such atmospheric changes. However, relative humidity or variations in both air temperature and specific humidity are more important for the generation of convection under conditionally unstable atmospheric conditions.

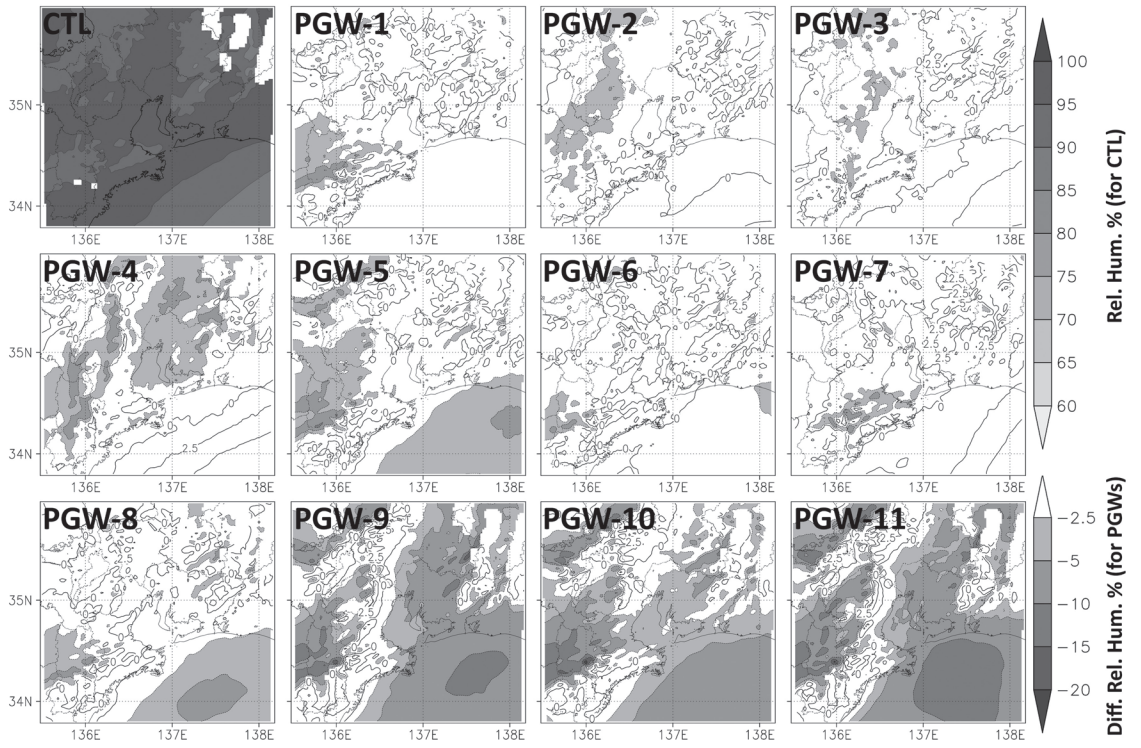

Fig. 12. Spatial distributions of 850 hPa relative humidity in CTL and difference of relative humidity between each PGW and CTL. Results are averaged over the period from 15:00 JST 11 September to 09:00 JST 12 September and five ensemble members. Upper color bar is for relative humidity of CTL and lower bar is for difference of relative humidity between each PGW and CTL. Color bars shows relative humidity (%).

6. Summary

In this study, we performed a hindcast of the THR in 2000 and investigated possible changes to this extreme event under future climate conditions using the PGW method. In the hindcast and each future simulation of 11 PGW runs, five ensemble members were prepared by the LAF method to examine whether the differences between simulations were caused by chaotic behaviors or global warming.

In the THR hindcast, the rainfall distribution around the Japanese islands was similar among the ensemble members, and effects of chaotic behaviors appeared weak in the meso-α scale rainfall system. In the model domain surrounding the Tokai region, there was a rain area from the Kii Peninsula to Nagoya. There were similar characteristics in the actual rainfall distribution of RAP. However, the area of heavy rainfall shifted slightly northward, and the location and extent of the area is different between ensemble members. The rainfall system developed around the frontal zone between warm and cold air masses, and was advected by upper-level winds in the simulations. A rainband was formed and maintained by such atmospheric conditions, and a back- and side-building type rainfall system described in previous studies was reproduced.

In the future PGW runs, heavy rain events similar to the CTL were produced around the Tokai region. However, in some cases, the heavy rainfall area was displaced northward. Among ensemble members in each PGW run, some similarities were found in rainfall distributions around Japan. These results indicate that effects of chaotic behaviors are expected to be small, and global warming mainly caused the difference between the PGW and CTL runs. In the cases of heavy rainfall in the region, the maximum hourly precipitation rate tended to increase in the future. Heavy rain over short periods may occur over wider areas in future climate. There was a wide variety in the maximum total and hourly precipitation among five ensemble members in the CTL and PGW runs.

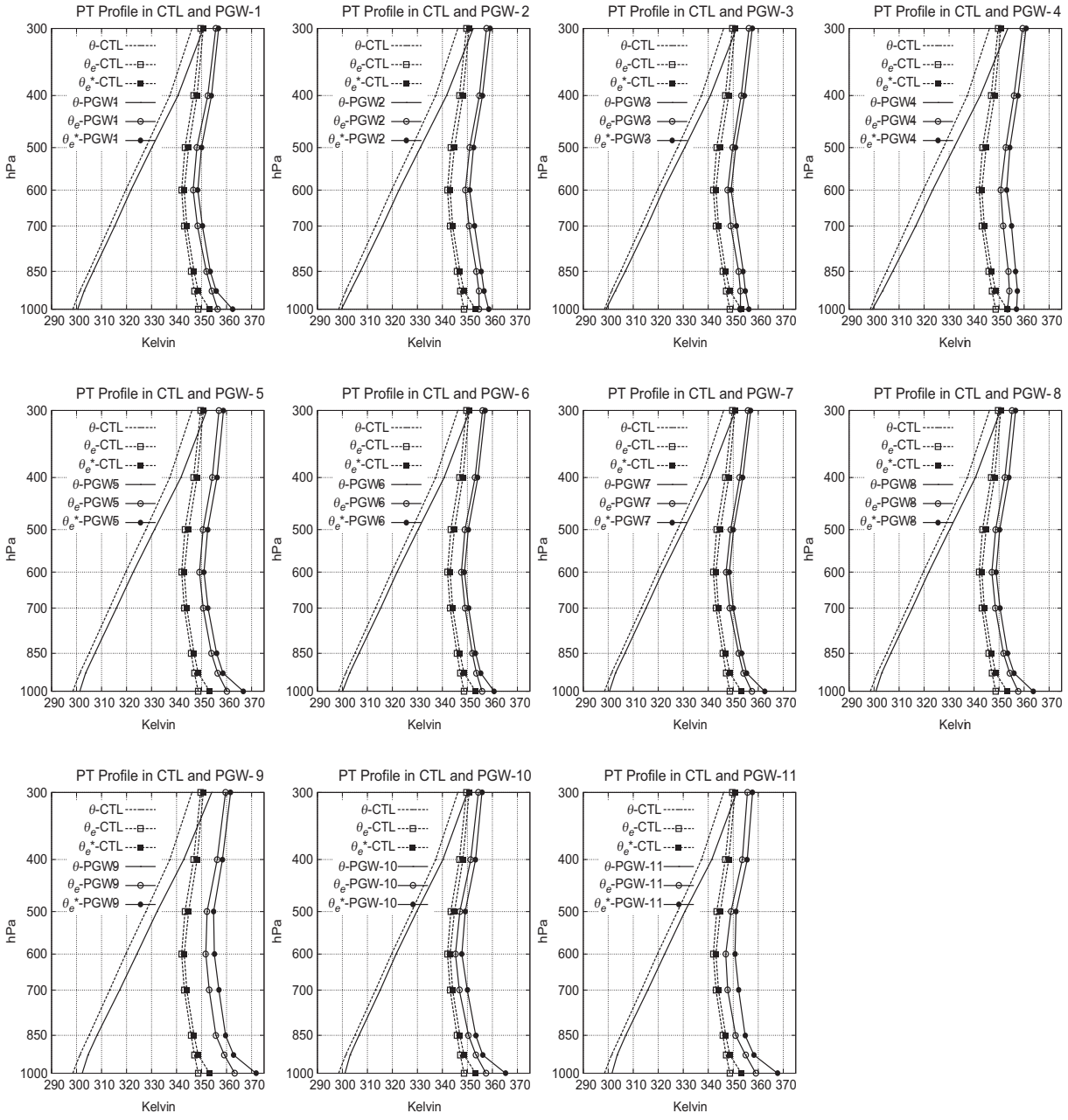

Fig. 13. Vertical profiles of potential temperature (θ), equivalent potential temperature (θ_e), and saturated equivalent potential temperature (θ_e^*). Dashed lines are results of CTL and solid lines of PGW runs. Values are averaged for the area of 136.2°–137.7°E, 34.6°–35.4°N and five ensemble members. Vertical axis is pressure height (hPa). Horizontal axis is temperature (K).

These results demonstrate the importance of ensemble simulations.

Some PGW runs produced an absence of significant rainfall around the Tokai region. In these runs, the spatial distribution of air temperature was similar to the PGW runs with heavy rainfall, and the specific humidity increased. However, these conditions were not sufficient to generate convection and heavy rainfall. Atmospheric vertical profiles showed a conditionally unstable stratification in these PGW runs, but

relative humidity was reduced; therefore, this was not conducive to convective development. Thus, when assessing heavy rainfall from convection in future climate, the relationship between air temperature and humidity must be investigated in detail.

Aside from the THR in 2000, the same type of heavy rain events have occurred in the Tokai region. It is important to study future rainfall events under synoptic-scale conditions similar to those of THR. Thus, the simulations with PGW conditions are very useful. The accumulation of simulations with PGW conditions for the Tokai region will clarify future changes of heavy rainfall. In our study, there were only five members for each ensemble of CTL and PGW. Increasing the number of ensemble members facilitates statistical approaches for evaluating future variations of individual extreme weather events.

There were significant differences in precipitation around a typhoon between the CTL and PGW runs. PGW DDS is anticipated to be of great help for assessment of future typhoon variations.

We used the CMIP3 dataset but using the new global warming experiment (CMIP5) data should reduce uncertainty in global warming experiments. We also used the Special Report on Emissions Scenario A1B, but applications for different scenarios are necessary to address possible variations in future climate. For local weather phenomena, considering future variations of land use is also important. Regarding the THR, SST in Ise Bay was believed to affect the formation and development of precipitation systems. However, SST was given as a boundary condition, and interactions between atmosphere and ocean were not simulated. In high-resolution assessments of climate change effects on local meteorological phenomena, evaluations of such uncertainties remain as challenges.

Acknowledgments

The authors are grateful for use of CMIP3 products archived and published by the Program for Climate Model Diagnosis and Intercomparison (PCMDI) and to all research institutes contributing to this activity. The GPCP precipitation data were provided by NASA/Goddard Space Flight Center's Laboratory for Atmospheres, and the Japanese 55-Year reanalysis data were provided by the Japan Meteorological Agency (JMA) and Central Research Institute of Electric Power Industry (CRIEPI). This research was supported through Core Research for Evolutional Science and Technology (CREST), funded by the Japan Science and Technology Agency (JST). The authors also greatly appreciate anonymous reviewers for their helpful comments and suggestions to improve the quality of the paper.

References

Bretherton, C. S., and S. Park, 2009: A new moist turbulence parameterization in the Community Atmosphere Model. *J. Climate*, **22**, 3422–3448.

Chang, E. K. M., Y. Guo, and X. Xia, 2012: CMIP5 multimodel ensemble projection of storm track change under global warming. *J. Geophys. Res.*, **117**, D23118, doi:10.1029/2012JD018578.

Chen, F., and J. Dudhia, 2001: Coupling an advanced land surface-hydrology model with the Penn State-NCAR MM5 modeling system. Part I: Model implementation and sensitivity. *Mon. Wea. Rev.*, **129**, 569–585.

Courtier, P., J.-N. Thepaut, and A. Hollingsworth, 1994: A strategy for operational implementation of 4D-Var, using an incremental approach. *Quart. J. Roy. Meteor. Soc.*, **120**, 1367–1387.

Emanuel, K., R. Sundararajan, and J. Williams, 2008: Hurricanes and global warming: Results from downscaling IPCC AR4 simulations. *Bull. Amer. Meteor. Soc.*, **89**, 347–367.

Hoffman, R. N., and E. Kalnay, 1983: Lagged average forecasting, and alternative to Monte Carlo forecting. *Tellus A*, **35**, 100–118.

Huffman, G. J., R. F. Adler, M. Morrissey, D. T. Bolvin, S. Curtis, R. Joyce, B. McGavock, and J. Susskind, 2001: Global precipitation at one-degree daily resolution from multi-satellite observations. *J. Hydrometeor.*, **2**, 36–50.

Iacono, M. J., J. S. Delamere, E. J. Mlawer, M. W. Shephard, S. A. Clough, and W. D. Collins, 2008: Radiative forcing by long-lived greenhouse gases: Calculations with the AER radiative transfer models. *J. Geophys. Res.*, **113**, D13103, doi:10.1029/2008JD009944.

IPCC, 2013: *Climate Change 2013: The Physical Science Basis*. Cambridge University Press, 1535 pp.

Janjic, Z. I., 1994: The step-mountain Eta coordinate model: Further development of the convection, viscous sublayer, and turbulence closure scheme. *Mon. Wea. Rev.*, **122**, 927–945.

Janjic, Z. I., 2000: Comments on "development and evaluation of a convection scheme for use in climate models". *J. Atmos. Sci.*, **57**, 3686–3686.

Kato, T., 2002: Modeling and forecast of heavy rainfall – Approach with numerical models –. *Tenki*, **48**, 626–634 (in Japanese).

Kawase, H., T. Yoshikane, M. Hara, B. Ailikun, F. Kimura, and T. Yasunari, 2008: Downscaling of the climatic changes in the Mei-yu rainband in East Asia by a pseudo climate simulation method. *SOLA*, **4**, 73–76.

Kawase, H., T. Yoshikane, M. Hara, F. Kimura, T. Yasu-

nari, B. Ailikun, H. Ueda, and T. Inoue, 2009: Inter-model variability of future changes in the baiu rain-band estimated by the pseudo global warming down-scaling method. *J. Geophys. Res.*, **114**, D24110, doi:10.1029/2009JD011803.

Kim H.-S., G. A. Vecchi, T. R. Knutson, W. G. Anderson, T. L. Delworth, A. Rosati, F. Zeng, and M. Zhao, 2014: Tropical cyclone simulation and response to CO_2 doubling in the GFDL CM2.5 high-resolution coupled climate model. *J. Climate*, **27**, 8034–8054.

Knutti, R., and J. Sedláček, 2013: Robustness and uncertainties in the new CMIP5 climate model projections. *Nat. Climate Change*, **3**, 369–373.

Kobayashi, S., Y. Ota, Y. Harada, A. Ebita, M. Moriya, H. Onoda, K. Onogi, H. Kamahori, C. Kobayashi, H. Endo, K. Miyaoka, and K. Takahashi, 2015: The JRA-55 Reanalysis: General specifications and basic characteristics. *J. Meteor. Soc. Japan*, **93**, 5–48.

Kusaka, H., M. Hara, and Y. Takane, 2012: Urban climate projection by the WRF model at 3-km horizontal grid increment: Dynamical downscaling and predicting heat stress in the 2070's August for Tokyo, Osaka, and Nagoya metropolises. *J. Meteor. Soc. Japan*, **90B**, 47–63.

Meehl, G. A., C. Covey, T. Delwarth, M. Latif, B. McAvaney, J. F. B. Mitchell, R. J. Stouffer, and K. E. Taylor, 2007: The WCRP CMIP3 multimodel dataset: A new era in climate change research. *Bull. Amer. Meteor. Soc.*, **88**, 1383–1394.

Morrison, H., G. Thompson, and V. Takarskii, 2009: Impact of cloud microphysics on the development of trailing stratiform precipitation in a simulated squall line: Comparison of one- and two-moment schemes. *Mon. Wea. Rev.*, **137**, 991–1007.

Murakami, H., B. Wang, and A. Kitoh, 2011: Future changes of western north pacific typhoons: Projections by a 20-km-mesh global atmospheric model. *J. Climate*, **24**, 1154–1169.

Nakicenovic N., and R. Swart, 2000: IPCC special report. Emission Scenario. Cambridge University Press, 570 pp.

NCEP, 2000: NCEP FNL Operational model global tropospheric analyses, continuing from July 1999. *Research Data Archive at the National Center for Atmospheric Research, Computational and Information Systems Laboratory*, Boulder, CO. [Available at http://dx.doi.org/10.5065/D6M043C6.]

Oouchi, K., J. Yoshimura, H. Yoshimura, R. Mizuta, S. Kusunoki, and A. Noda, 2006: Tropical cyclone climatorogy in a global-warming climate as simulated in a 20km-mesh global atmospheric model: Frequency and wind intensity analysis. *J. Meteor. Soc. Japan*, **84**, 259–279.

Pielke, Jr., R. A., C. Landsea, M. Mayfield, J. Laver, and R. Pasch, 2005: Hurricanes and global warming. *Bull. Amer. Meteor. Soc.*, **86**, 1571–1575.

Reynolds, R. W., T. M. Smith, C. Liu, D. B. Chelton, K. S. Casey, and M. G. Schlax, 2007: Daily high-resolution blended analysis for sea surface temperature. *J. Climate*, **20**, 5473–5496.

Sato, T., F. Kimura, and A. Kitoh, 2007: Projection of global warming onto regional precipitation over Mongolia using a regional climate model. *J. Hydrol.*, **333**, 144–154.

Scoccimarro, E., S. Gualdi, G. Villarini, G. A. Vecchi, M. Zhao, K. Walsh, and A. Navarra, 2014: Intense precipitation events associated with landfalling tropical cyclones in response to a warmer climate and increased CO_2. *J. Climate*, **27**, 4642–4654.

Skamarock, W. C., J. B. Klemp, J. Dudhia, D. O. Gill, D. M. Barker, M. G. Duda, X.-Y. Huang, W. Wang, and J. G. Powers, 2008: *A description of the advanced research WRF version 3*. NCAR Technical Note, NCAR/TN-475+STR, 113 pp.

Watanabe, S., 2002: Observation and analysis of heavy rainfall in Tokai. *Tenki*, **48**, 609–619 (in Japanese).

Webster, P. J., G. J. Holland, J. A. Curry, and H.-R. Chang, 2005: Changes in tropical cyclone number, duration, and intensity in a warming environment. *Science*, **309**, 1844–1846.

Yokoi, S., and Y. N. Takayabu, 2009: Multi-model projection of global warming impact on tropical cyclone genesis frequency over the western north Pacific. *J. Meteor. Soc. Japan*, **87**, 525–538.

Zappa, G., L. C. Shaffrey, K. I. Hodges, P. G. Sansom, and D. B. Stephenson, 2013: A multimodel assessment of future projections of North Atlantic and European extratropical cyclones in the CMIP5 climate models. *J. Climate*, **26**, 5846–5862.

Zilitinkevich, S. S., 1995: Non-local turbulent transport: Pollution dispersion aspects of coherent structure of convective flows. *Air Pollution III, Volume I, Air pollution theory and simulation*. Power, H., N. Moussiopoulos, and C. A. Brebbia (eds), Computational Mechanics Publications, Southampton, Boston, 53–60.